

# Continuum and Atomistic Modeling of Ion Partitioning into a Peptide Nanotube

D. Asthagiri and D. Bashford

Department of Molecular Biology, TPC-15, The Scripps Research Institute, La Jolla, California 92037 USA

**ABSTRACT** Continuum and atomistic descriptions of the partitioning of ions into a self-assembled (D,L)-octapeptide nanotube, cyclo[-(L-Ala-D-Ala)<sub>4</sub>-], are presented. Perturbation free energy calculations, including Ewald electrostatics, are used to estimate the electrostatic component of the excess free energy of charging Li<sup>+</sup>, Na<sup>+</sup>, Rb<sup>+</sup>, and Cl<sup>-</sup> ions inside the nanotube. The radial density and orientational distribution of water around the ion is calculated for the ion at two different positions inside the tube; it is seen that the calculated distributions are sensitive to the location of the ions. Two different continuum electrostatic models are formulated to describe the ion solvation inside the nanotube. When enhanced orientational structuring of water dipoles is evidenced, explicitly including the first solvation shell as part of the low dielectric nanotube environment provides good agreement with molecular dynamics simulations. When water orientational structuring is as in the reference bulk solvent, we find that treating the first shell water explicitly or as a high dielectric continuum leads to similar results. These results are discussed, and their importance for continuum electrostatic modeling of ion channels are highlighted.

## INTRODUCTION

Synthetic ion channels are emerging as promising nanoscale biosensor devices (Bayley, 1999; Hartgerink et al., 1998), and self-assembled channels of the kind considered in this paper have demonstrated potent antibacterial properties (Fernandez-Lopez et al., 2001). The ease of introducing and evaluating design changes in synthetic systems provides an opportunity to test computational models of ion channels, thus advancing the quantitative understanding of analogous biological systems. The present study is guided by this aim. An earlier work addressed via molecular dynamics (MD) simulations the dynamics of water in a self-assembled, cyclo[-(L-Gln-D-Ala-L-Glu-D-Ala)<sub>2</sub>-] octapeptide nanotube (Engels et al., 1995). In the present investigation, we use both MD and continuum electrostatics to study the energetics of transferring an ion from the bulk to specified locations inside a nanotube comprising cyclo[-(L-Ala-D-Ala)<sub>4</sub>-] monomers.

Molecular dynamics has been extensively used in biomolecular simulations, and the exemplar of this technique for channel systems are the investigations by Roux and Karplus (1991, 1993), who used an atomic description of the channel, water, and ions to study the translocation of water and alkali metal ions through gramicidin. (See, for example, Hao et al. (1997) and Åqvist and Luzhkov (2000) for more recent applications of MD in calculating ion translocation energetics through biological channels.) Although MD is now routinely used in biomolecular simulation, it still requires a significant investment of time and computational

resources. For example, realistic membrane-protein simulations such as those reported by Tieleman and Berendsen (1998) or Bernèche and Roux (2000) are still much too computationally intensive to be used on a routine basis. Furthermore, if one is interested not in the actual dynamics but only the energetics of placing an ion inside an ion channel, and if this estimate is required for a number of different modifications of the channel, then simplified alternatives to MD become desirable.

The use of non-MD approaches to study ion partitioning in channel systems has not been as extensive. Åqvist and Warshel (1989) studied ion translocation through the gramicidin channel using the protein-dipole Langevin-dipole formulation for the channel protein, membrane, and bulk water but used explicit water molecules inside the channel itself. They were able to obtain activation barriers that were in reasonable agreement with experimental estimates. Jordan and coworkers have pursued a more reduced, semimicroscopic description of channels (Partenskii and Jordan, 1992a,b; Partenskii et al., 1994; Sancho et al., 1995): the atomistic protein structure was disregarded, the water external to the channel was treated as a high dielectric continuum, whereas the water inside the channel was represented by freely rotating dipoles. Using this description, they illustrated the nonlinearity of the electric response upon the introduction of an ion into the channel. In a recent study, Roux and MacKinnon (1999) investigated the selectivity of a KcsA (K<sup>+</sup>) channel using continuum electrostatics and were able to show how the ion is stabilized in the low dielectric protein/membrane environment.

In this work we present atomistic MD simulations of ion-channel systems and formulate computationally facile continuum electrostatics models based on insights gleaned from the simulations. The model channel is a self-assembled cyclic octapeptide with an alternating (D,L)-amino acid sequence (Hartgerink et al., 1998; Ghadiri et al., 1994). These

*Submitted May 15, 2001, and accepted for publication December 5, 2001.*

Address reprint requests to Dr. Donald Bashford, The Scripps Research Institute, Department of Molecular Biology, 10550 North Torrey Pines Road, La Jolla, CA 92037. Tel.: 858-784-9612; Fax: 858-784-8896; E-mail: bashford@scripps.edu.

© 2002 by the Biophysical Society

0006-3495/02/03/1176/14 \$2.00

cyclic peptides self-assemble into a cylindrical tube with a  $\beta$ -sheet (backbone) architecture. The nanotube channel provides a more complicated, yet experimentally accessible, system compared with gramicidin. Like gramicidin, the nanotube is made of alternating (D,L)-amino acids. Further, like gramicidin (Arseniev et al., 1985), the nanotube pore wall is solely lined by carbonyl and amide dipoles. However, there is one critical difference, the nanotube pore diameter of  $\sim 6$  Å is twice that of gramicidin. (These pore diameters were estimated with Oliver Smart's HOLE program (Smart et al., 1993).) Thus, unlike gramicidin, the nanotube channel contains more than a single column of water molecules (Engels et al., 1995), and the ion can, in principle, coordinate with more than two water molecules, which is the maximum possible in the gramicidin channel. The larger diameter also leads to cation conduction rates about three times greater (Ghadiri et al., 1994) than that in gramicidin. The pore diameter of the nanotube falls in the middle of the range of diameters noted for the nicotinic acetylcholine receptor channel, which has a pore diameter ranging between 3 Å to  $\sim 9$  Å (Opella et al., 1999) and a greater variety of groups lining the pore.

We study the water-tube transfer energetics of  $\text{Li}^+$ ,  $\text{Na}^+$ ,  $\text{Rb}^+$ , and  $\text{Cl}^-$ , initially using MD-based perturbation free energy methods, thereby exploring the solvation structure and thermodynamics of particles with a range of sizes and charge. To better study the structure and thermodynamics of ion solvation in nanotubes, we focus exclusively on the solvation of a solitary ion inside the channel. An important aspect of our work is the treatment of long-range electrostatic interactions using Ewald summation. To the best of our knowledge, this is the first study to use perturbation free energy simulations including Ewald-electrostatics for ions in nanotubes. Earlier investigations of channel systems have typically used various truncation schemes to study the dynamics and energetics of ion transport (but see Bernéche and Roux (2000)). We find that the structuring of water molecules around the ion is sensitive to the location of the ion inside the channel. We present macroscopic models at various levels of detail and highlight the interrelation of water structuring and continuum modeling. Water structuring should manifest as a nonlinearity of the medium's electrostatic response; however, we find it difficult to unequivocally discern water structuring based solely on the calculated electrostatic response. The possible reasons for this are discussed. The present work demonstrates the subtlety and importance of water structuring in the narrow confines of ion channels and provides ways to describe these effects in continuum electrostatics calculations.

## THEORY AND METHODS

Molecular dynamics simulations were performed with the CHARMM (Brooks et al., 1983) molecular mechanics package (version c26b2) using the all-atom PARAM22 forcefield (MacKerell et al., 1998). The Lennard-

Jones parameters for  $\text{Na}^+$  and  $\text{Cl}^-$  are from Beglov and Roux (1994), and those for  $\text{Li}^+$  and  $\text{Rb}^+$  are from Åqvist (1990). The  $\text{Li}^+$  and  $\text{Rb}^+$  parameters, originally used with the simple point charge water model (Åqvist, 1990), were used with the TIP3P (Neria et al., 1996; Jorgensen et al., 1983) water model in CHARMM. (In CHARMM, the water protons have a small radius as opposed to the original TIP3P (Jorgensen et al., 1983) water model.)

The continuum electrostatics calculations were performed with the MEAD (Macroscopic Electrostatics with Atomic Detail) (Bashford and Gerwert, 1992; Bashford, 1997) suite of programs. The atomic partial charges from the PARAM22 forcefield and the corresponding atomic radii compiled by Nina et al. (1997) were used. The Born radii of the ions used in the MEAD calculations were determined from simulations as discussed below.

## Molecular structure

The cyclic octapeptide  $c(\text{DAA})_4$  used in this study is a simplification of the  $c(\text{DLW})_4$  octapeptide used experimentally (Sanchez-Quesada and Ghadiri, personal communication; see also Ghadiri et al., 1994; Motesharei and Ghadiri, 1997). The monomer  $c(\text{DAA})_4$  peptide was made from a D-Ala-L-Ala dimer by applying a fourfold rotation about the  $z$  axis. Initial bond lengths and bond angles in the D-Ala-L-Ala dimer were taken from the equilibrium bond lengths and bond angles of the PARAM22 forcefield (MacKerell et al., 1998). Initial dihedral angles were taken from the crystal structure of the blocked octapeptide dimer  $c(\text{LWDA})_4$  (Ghadiri et al., 1993). This cyclic peptide was energy minimized by the adopted basis Newton-Raphson (ABNR) method, which was carried to convergence; the fourfold symmetry was maintained during the energy minimization.

To create an octapeptide dimer having a backbone structure matching, as closely as possible, the experimental crystal structure, a duplicate of the octapeptide was generated, rotated by  $180^\circ$  about a line passing through the  $\alpha$ -carbon atoms of residues 1 and 5, translated by  $-5.006$  Å along the  $z$  axis and finally rotated by  $9.17^\circ$  about the  $z$  axis. The resulting octapeptide dimer was energy minimized using the ABNR method. The energy minimization was carried out in a symmetrical infinite-tube environment generated by translating dimer images  $\pm 9.4$  Å along the  $z$  axis. The  $9.4$  Å was arrived at by a series of similar energy minimizations using different  $z$  translations from which it was found that  $9.4$  Å gave the lowest final energy. Crystallographic studies of the blocked dimer suggest a unit cell dimension of  $\sim 4.7$  Å (Ghadiri et al., 1993) corresponding to a dimer translation of  $\sim 9.4$  Å, in good agreement with what we find via the energy-minimization protocol.

From this energy-minimized octapeptide dimer, a 4-mer nanotube was created in two stages. First the octapeptide dimer was filled with a canonical count of water (Engels et al., 1995): one water molecule in each  $\alpha$ -plane, and two water molecules in each midplane (Fig. 1). This dimer was energy minimized in a symmetrical-infinite environment. Second a 4-mer nanotube was built from this energy-minimized, water-filled dimer by appropriate translational symmetry operations. The choice of a 4-mer nanotube is made for computational convenience. In experiments the tube length would depend on the bilayer used, which for a DMPC bilayer would amount to having six to eight monomers, based on the intermonomer spacing of  $\sim 5$  Å.

## Molecular dynamics

The water-filled nanotube is solvated in a preequilibrated box of TIP3P (Neria et al., 1996; Jorgensen et al., 1983) water molecules. Any water molecules external to the nanotube whose oxygen atoms were closer than  $2.8$  Å were deleted as overlapping waters. A  $\text{Na}^+$  ion was placed in the midplane region bounded by  $\alpha$ -planes B and C (Fig. 1). The volume of this system was adjusted based on a partial specific volume of  $1$  cc/gm for water and ion and  $0.73$  cc/gm for the nanotube (Engels et al., 1995).

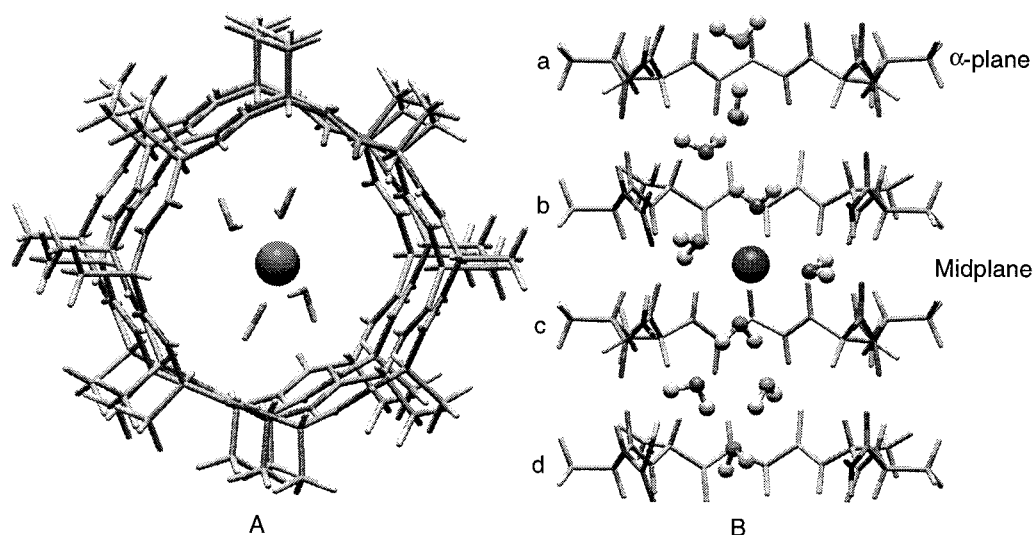


FIGURE 1 Schematic of the 4-mer. The  $\alpha$ -plane of each monomer is defined as the plane coming closest (in the least square sense) to passing through the  $\alpha$ -carbon atoms of the monomer. The midplanes are defined as the planes midway between the  $\alpha$ -planes. (A) Slightly off-center view along the axis of the channel. Only the innercoordination shell of the ion is shown for clarity. (B) View perpendicular to the channel axis. The front of the channel has been cut away for clarity. The water molecules are arranged in a canonical fashion: two water molecules in the midplane and one in the  $\alpha$ -plane.

Overlaps with the internal water molecules were removed by minimization. The system so generated measures  $32.3 \text{ \AA} \times 32.3 \text{ \AA} \times 47.07 \text{ \AA}$  and comprises 320 nanotube atoms, 1549 water molecules, and the sole ion. In the initial course of this investigation we used this large simulation volume. However, comparable accuracy is obtained even with a small box that is derived from this system by deleting selected water molecules to give a cubic box with edge length  $28.948 \text{ \AA}$ . This smaller system comprises the nanotube, ion, and 718 water molecules. From this initial configuration, three additional boxes were obtained by replacing the  $\text{Na}^+$  ion with  $\text{Li}^+$ ,  $\text{Rb}^+$ , and  $\text{Cl}^-$  ions, respectively, followed by 50 steps of ABNR minimization. The four boxes thus obtained were the starting configurations for further studies.

In the initial phase of equilibration, each of the systems obtained above were equilibrated for more than 120 ps. During the equilibration cycle and for the rest of the simulation, the tube backbone atoms, i.e., the N (imino),  $\alpha$ -carbon, and carbonyl-carbon atoms were restrained with a harmonic (Hookian) spring of force constant  $2m \text{ kcal/mol-\AA}^2$ , in which  $m$  is the mass of the respective atom in atomic mass units. The ion was held in place by a harmonic spring of force constant  $10m \text{ kcal/mol-\AA}^2$ . Dynamics were propagated using the Leapfrog Verlet (Allen and Tildesley, 1997) algorithm using a time step of 1 fs. The SHAKE (Ryckaert et al., 1977) algorithm was used to rigidly fix bonds to hydrogen atoms. The temperature was maintained at 298 K by coupling to a heat bath with a coupling constant of 0.5 ps (Berendsen et al., 1984). The nonbonded interaction list was truncated at  $12 \text{ \AA}$  on an atom basis; the van der Waals interactions were switched to zero from  $10 \text{ \AA}$  to  $12 \text{ \AA}$ ; and Ewald sums with conducting boundary conditions were used for electrostatic interactions with the Ewald damping coefficient  $\eta$  set to  $0.2333 \text{ \AA}^{-1}$ . The reciprocal space cutoff was determined by performing test calculations to determine a suitable value. This lead to a spherical cutoff such that  $\kappa^2 \leq 38(2\pi/L)^2$ .  $\vec{\kappa}$ , the reciprocal space lattice vector, is given by  $\vec{\kappa} = 2\pi(l/L_x, m/L_y, n/L_z)$  (Feller et al., 1996), in which  $L_x$ ,  $L_y$ , and  $L_z$  are the box dimensions. Because the Ewald formulation is meaningful only for a neutral system, a uniform background compensating charge density is added to ensure electroneutrality of the simulation cell. This charge density is just the negative of the net charge smeared over the entire simulation volume. (The interested reader should consult Tosi's (1964) clear presentation of Ewald summation in the presence of a neutralizing background.)

In the next phase of equilibration, the ion charge was slowly changed from the full formal charge to zero charge as follows. A series of equilibrated trajectories with ion charges of  $q\lambda$  ( $q = \pm 1 \text{ a.u.}$ ;  $\lambda = 0.95, 0.85, \dots, 0.05$ ) were generated, in which the starting configuration of each trajectory was taken from the final configuration of the earlier trajectory. For example, the  $\lambda = 0.85$  trajectory began with the ending coordinates of the  $\lambda = 0.95$  trajectory. For each of the trajectories, initial velocities were assigned from a Gaussian distribution such that the initial temperature was 625 K. By scaling the particle velocities, the systems were cooled to 298 K over 1 ps followed by 1 ps of equilibration with temperature maintained at 298 K by velocity rescaling. This "scrambling" of water configuration was primarily to prevent water molecules from getting trapped in some particular configuration, as this is a matter of concern when the water molecules are confined to a narrow channel. These systems were further equilibrated for 8 ps with temperature maintained at 298 K by coupling to a heat bath. The nonbonded interactions were treated as mentioned above. The end point of the  $\lambda = 0.05$  trajectory was taken as the starting point for subsequent perturbation free energy calculations. We adopted this approach to minimize hysteresis in subsequent perturbation calculations, as the present approach would likely ensure that the all-important water configuration around the ion is not trapped in a state corresponding to the ion at a higher charge state. This is validated by the modest error bars on the calculated free energies (Results section). Note that the perturbation free energy calculations were done in two different ways. As discussed below, one method for calculating the free energy incorporated the "scrambling" of water at each charge state  $\lambda$ ; the other did not, but the simulation extended for much longer, namely 300 ps.

The starting configuration for the simulations with the ion in the  $\alpha$ -plane was obtained via a somewhat different protocol. We used the small  $28.948 \text{ \AA}$  simulation box from the very start, instead of using a bigger box and deleting water molecules. The ion was inserted in  $\alpha$ -plane B (Fig. 1) and the ion and tube atoms restrained as before. This system was equilibrated for 200 ps using a 2-fs timestep, followed by a 300-ps perturbation free energy calculation, again using a 2-fs time step. Bonds to hydrogen atoms were fixed using SHAKE (Ryckaert et al., 1977). The charge was turned off in steps of 0.05, to obtain the  $\lambda = 0.05$  state. At each step a 10-ps equilibration was followed by 20 ps of data collection. Thus, this procedure of obtaining the  $\lambda = 0.05$  state also provided an estimate of the discharging

free energy (data not shown). All subsequent perturbation calculations for the ion in the  $\alpha$ -plane were as for the ion in the midplane, i.e., using a 1-fs timestep and included a “scrambling” at each charge state. Likewise a few 300-ps charging perturbation calculations using a 2-fs timestep were performed for the ion in the midplane (data not shown). Adopting different styles of perturbation and different timesteps permitted us to evaluate the effect of these variables on calculated numbers. The average energetic values obtained using the 300-ps perturbation calculations (data not shown) are similar to the values reported in this work indicating that the calculations are reasonably well converged.

### Solvation energetics

Perturbation free energy calculations were carried out using the PERT module in CHARMM. Briefly, if the two states of the system have the potential energies  $E(1)$  and  $E(2)$ , then the free energy change in going from state 1 to state 2 is given by

$$\Delta A = -k_B T \ln \left\langle \exp \left( - \frac{E(2) - E(1)}{k_B T} \right) \right\rangle_{(1)} \quad (1)$$

where the ensemble is generated at state 1 and  $k_B$  is the Boltzmann constant (Zwanzig, 1954; Beveridge and DiCupua, 1989). Although the formula as written is exact, it is useful only when the states 1 and 2 are not much different. Thus, in practice, the interval between states 1 and 2 is further subdivided and the free energy change computed as

$$\Delta A = \sum_{i=1}^n \Delta A(\lambda_{i \rightarrow i+1}) \quad (2)$$

where the index  $i$  specifies the respective state, and there are a total of  $n + 1$  states.  $\lambda$  is a parameter that couples  $E(2)$  and  $E(1)$  by the formula  $E(\lambda) = E(1) \cdot \lambda + E(2) \cdot (1 - \lambda)$ . In the present study,  $\lambda$  couples the state where the ion is fully charged to the state with an ion charge of zero. Thus we calculate only the purely electrostatic contributions of solvation, which are the most dominant for charged species.

It is important to highlight aspects of the Ewald summation pertinent to free-energy simulations. The presence of the neutralizing charge density and the presence of the periodic copies of the source charge leads to a potential at the source charge, the so-called Wigner potential (Hummer et al., 1996). For a charge  $q$  this potential is  $q\xi$ , where  $\xi \approx -2.837297/L$  for a cubic simulation box of side  $L$ . The presence of this potential leads to a self-interaction term that must be included to remove electrostatic finite-size effects (Hummer et al., 1996). Hence the free energy change in going from charge state  $q_i$  to  $q_{i+1}$  can be written as (Hummer et al., 1996):

$$\Delta A_{i \rightarrow i+1} = \Delta A_{i \rightarrow i+1}(\text{uncorr}) + \frac{1}{2} \xi (q_{i+1}^2 - q_i^2) \quad (3)$$

in which  $\Delta A(\text{uncorr})$  is the free energy change without the self-interaction correction. The second term in Eq. 3 is the self-interaction (finite-size) correction, which was properly accounted for in our simulations.

Starting from the  $\lambda = 0.05$  state, equilibrated structures were generated with ion charges of  $q\lambda$  ( $q = \pm 1$  a.u.;  $\lambda = 0.05, 0.15, \dots, 0.95$ ) to serve as starting points for subsequent charging free energy calculations over the range  $\lambda = 0.0$  to  $0.1$ ,  $0.1$  to  $0.2$ , etc. The starting coordinates for equilibration trajectories at various  $\lambda_i$  values were generated as in the initial equilibration runs for ion in the midplane; for example, the  $\lambda = 0.25$  trajectory was generated starting from the end-point of the equilibration phase of the  $\lambda = 0.15$  trajectory, and this included a 2-ps “scrambling” run and an 8-ps equilibration run. Trajectories for a further 10 ps beyond the equilibration phases were propagated, and free energy differences were calculated by perturbing the charge by  $\pm 0.05q$  ( $\lambda = \pm 0.05$ ), i.e., by a double-wide sampling (for example, see Beveridge and DiCupua, 1989) at each  $\lambda$ . Thus, in total, 200 ps of simulations were performed for evaluating

the charging free energy,  $\Delta A_{\text{tube}}$ , of each ion inside the tube. This protocol was followed for all ionic species and for both midplane and  $\alpha$ -plane positions.

Simulations were also conducted in the opposite direction, i.e., the ion charge was decreased. In this case the equilibrated  $\lambda = 0.95$  state obtained above in the charging phase of the calculation was used to successively generate states with lower charge as described earlier. At each  $\lambda$ , an additional 10 ps of trajectory was generated to evaluate the discharging free energy. The average of the charging and discharging steps gave the electrostatic component of the free energy of (dis)charging the ion inside the nanotube.

Perturbation calculations were performed in bulk water to provide the reference-state excess free energy,  $\Delta A_{\text{bulk}}$ , of the charging process. The ion was solvated in a cubic box of 216 water molecules at a density of 1 gm/cc. The nonbonded interaction list was truncated at 8.3 Å on an atom basis; the van der Waals interactions were switched to zero from 7.3 Å to 8.3 Å; and the Ewald summation used  $\eta = 0.337 \text{ Å}^{-1}$  and  $\kappa^2 \leq 27(2\pi/L)^2$ . For the thermodynamic perturbation studies, the coupling parameter  $\lambda$  was changed from 0.975 to 0.025 in steps of 0.05, and at each  $\lambda$ , the charge was perturbed by  $\lambda \pm 0.025$ . Similar runs were performed in the opposite direction to estimate the average free energy of solvation and also to obtain an estimate of errors.

### Solvation structure

To calculate the structural aspects of ion hydration inside the nanotube, additional trajectories were generated at charge states  $\lambda = 1$  and  $\lambda = 0.5$  respectively. The starting configurations for these were the  $\lambda = 0.95$  and  $\lambda = 0.55$  states generated in the charging run (above). These configurations were equilibrated for an additional 10 ps. Then an additional 20 ps of trajectory was generated, and coordinates were saved every 0.1 ps for further analysis.

The density distribution of water around the ion was calculated by binning the ion-oxygen (water) separation in intervals of 0.05 Å. The structural data was also analyzed to study the orientation of water around the ion. As a measure of orientational order, the cosine of the angle between the ion-oxygen vector and the water dipole vector was used. For example, if the Na-O (water) vector is collinear with the water dipole, the angle  $\theta$  is  $0^\circ$  ( $\cos \theta = 1$ ). Similarly, when Cl-H(water)-O(water) are collinear, the angle between vector Cl-O and the water dipole is  $127.75^\circ$  ( $\cos \theta = -0.61$ ). (The  $\angle \text{HOH}$  in TIP3P water is  $104.52^\circ$ .) The distribution of cosines was binned in intervals of 0.05, and the probability of observing a particular orientation,  $p(\cos \theta)$ , was calculated as the number of observation in a particular bin by the total number of observations. Only waters in the first shell were used in this analysis; the first shell is determined by the first minimum of the density distribution of water. Water structure and density distribution for ions in bulk water were likewise calculated. The simulations in bulk used 50 ps of equilibration at each  $\lambda$  value followed by 10-ps-long production runs. Coordinates were saved every 0.05 ps for further analysis. Separate programs were written to analyze the trajectories.

### Analysis of electrostatic response

In the thermodynamic integration approach (Straatsma and Berendsen, 1988; Hummer and Szabo, 1996), the change in the electrostatic component of the free energy in traversing from  $\lambda_1$  to  $\lambda_2$  is

$$\Delta A(\lambda_1 \rightarrow \lambda_2) = \int_{\lambda_1}^{\lambda_2} \left\langle \frac{\partial E}{\partial \lambda} \right\rangle_{\lambda} d\lambda = q \int_{\lambda_1}^{\lambda_2} \langle \psi \rangle_{\lambda} d\lambda \quad (4)$$

in which  $\langle \psi \rangle_{\lambda}$  is the mean potential at the ion at some charge state  $q\lambda$  ( $q = \pm 1$  a.u.). Because we have  $\Delta A(\lambda_i \rightarrow \lambda_{i+1})$  for various bins  $[\lambda_i, \lambda_{i+1}]$ ,  $\langle \psi \rangle$



(in units of kcal/mol-e) can be calculated via a finite difference approximation to numerical differentiation:

$$\langle\psi\rangle_{(\lambda_i+\lambda_{i+1})/2} = \frac{\Delta A(\lambda_i \rightarrow \lambda_{i+1})}{q \cdot (\lambda_{i+1} - \lambda_i)} \quad (5)$$

If the medium responds linearly,  $\langle\psi\rangle_\lambda \propto \lambda$ . Note that continuum theories based on the Poisson equation (see below) are linear response theories (Rick and Berne, 1994). An advantage of considering  $\langle\psi\rangle$ , i.e., the derivative of the free energy, is that any deviations from linearity are easily seen (Figueirido et al., 1994), whereas it is somewhat more difficult to perceive deviations from a quadratic behavior for  $\Delta A$  versus  $\lambda$ . Note again a consequence of the finite-size correction in Eq. 3. If the uncorrected free energy change in Eq. 3 is used in Eq. 5 above to obtain  $\langle\psi\rangle_\lambda(\text{uncorr})$ , the corrected potential would be given by  $\langle\psi\rangle_\lambda = \langle\psi\rangle_\lambda(\text{uncorr}) + \xi\lambda$ , which is what is presented in this work.

## Continuum electrostatics

The macroscopic description of ion solvation is based on treating the peptides and the bulk water as continua with dielectric constants of  $\epsilon = 4$  and  $\epsilon = 80$ , respectively. The ion with  $\epsilon = 1$  is represented as a spherical cavity with a charge at its center. The molecular surface (Connolly, 1983), determined by rolling a 1.4 Å radius probe sphere over the atomic radii, delineates regions of different dielectric constants. The potential is described by the Poisson equation, which must be solved numerically because of the complex shape of the dielectric boundaries. This is implemented with the above-mentioned MEAD software.

The electrostatic contribution to the excess free energy of the ion in the nanotube, with the ion in vacuum ( $\epsilon = 1$ ) as the reference state, is given by

$$\Delta A_{\text{tube}} = \frac{1}{2} q \psi_{\text{rxn}} + q \psi_{\text{channel}} \quad (6)$$

in which  $\psi_{\text{rxn}}$  is the reaction field acting on the ion in the multidielectric environment of the channel and the water with the all channel charges set to zero;  $\psi_{\text{channel}}$  is the potential at the position of the ion charge due to the peptide channel charges; and  $q$  is the charge of the ion itself.  $\psi_{\text{channel}}$  is independent of the ion charge, whereas  $\psi_{\text{rxn}}$  is proportional to the ion charge. Their sum,  $\psi_{\text{rxn}} + \psi_{\text{channel}}$ , is the continuum analog of  $\langle\psi\rangle_\lambda$  of Eq. 4. Here the  $\lambda$  dependence enters through the ion-charge dependence of  $\psi_{\text{rxn}}$ . Eq. 6 above for the ion in bulk water is just  $\Delta A_{\text{bulk}} = (\frac{1}{2})q\psi_{\text{rxn}}$ , where now  $\psi_{\text{rxn}}$  is  $q/a \cdot (1/\epsilon_0 - 1)$ , which is the Born model for ionic solvation. The factor of  $(\frac{1}{2})$  in Eq. 6 is simply a consequence of  $\psi_{\text{rxn}}$  depending linearly on charge.

The Poisson equation was solved by a finite difference approach as implemented in the MEAD (Bashford and Gerwert, 1992; Bashford, 1997) suite of programs. The initial coarse grid had 51 grid points with a grid spacing of 1 Å and the fine grid had 101 grid points with a grid spacing of 0.1 Å. Notationally we refer to this grid choice by  $51 \times 1:101 \times 0.1$ . We have also performed calculations at grid level  $51 \times 1:101 \times 0.25:111 \times 0.1$  with similar results.

Some of the macroscopic calculations included a limited number of solvation shell water molecules as part of the ion channel environment. In these cases, the assignment of water coordinates was performed as follows. Initial water coordinates were taken from the last frame of the MD simulation done in calculating the solvation structure. Water molecules not part of the first solvation shell were deleted and the nanotube coordinates reset to their original values, and the system was energy minimized (using ABNR) for 250 steps with the nanotube backbone and the ion harmonically restrained. Configurations with various fractional charge states were generated by energy minimization starting with the structure at the preceding charge state. Thus, for example, the structure corresponding to the  $\lambda = 0.75$  state was derived by energy minimization of the structure corresponding to  $\lambda = 1.0$ . We used this method as a means of allowing explicitly

**TABLE 1** Excess free energy (in kcal/mol) for charging the ion in bulk water and the associated Born radius (Å)

Ion	$\Delta A_{\text{Bulk}}$			
	Expt	Prior results	MD, this work	$a$ (Å)
Li <sup>+</sup>	−122.1*	−122.2*	−110.5	1.483
Na <sup>+</sup>	−98.2†	−105.1†	−93.5	1.754
Rb <sup>+</sup>	−75.5*	−75.5*	−67.1	2.443
Cl <sup>−</sup>	−80.0†	−80.0†	−94.8	1.729

$a$ , Born radius calculated using Eq. 7 and our charging free energy. The error bars, determined by averaging forward and backward simulations, are  $\sim 1$  kcal/mol and are not shown.

\*Calculated solvation free energies reported by Åqvist (1990).

†Solvation free energy values reported by Roux and coworkers (Beglov and Roux, 1994; Roux, 1996). The experimental values quoted by these authors are similarly highlighted. For Li<sup>+</sup>, Rb<sup>+</sup>, and Cl<sup>−</sup> the authors do not quote the purely electrostatic contribution to the free energy of charging, and hence these numbers are likely more positive by  $\sim 3$  kcal/mol, which is approximately the free energy of cavity creation for the ions under consideration.

included solvent shell water to respond to the charging process by explicit reorientation, while keeping the nanotube harmonically restrained, thus confining its response to that modeled by the dielectric constant of 4.

## RESULTS

### Molecular dynamics

The calculated excess free energies of charging the ions in the bulk solvent are presented in Table 1 along with experimental values and results of similar calculations by others. Because we are also interested in continuum electrostatic calculations, we relate the bulk hydration free energies obtained via microscopic simulations to their macroscopic counterpart, the Born model for ion solvation. This allows us to calculate the only free parameter in the Born model, the ionic radius, by the formula (Born, 1920),

$$\Delta A_{\text{bulk}} = \frac{166 \cdot q^2}{a} \left( \frac{1}{80} - 1 \right) \quad (7)$$

in which  $\Delta A_{\text{bulk}}$  is given in kcal/mol and  $q$  in atomic units, and  $a$  is the Born radius in Å. The radii thus obtained are intimately related to how water coordinates with the ion and are usually much different from the crystal (or Pauling) radii (for example, see Latimer et al., 1939). Molecular interpretations of the Born radius are usually based on the first peak of the ion-water radial distribution function (Roux et al., 1990) or an average of the crystal radius and the first-peak of the radial distribution function (Babu and Lim, 1999). In this study, together with the microscopic charging free energy calculation of  $\Delta A_{\text{bulk}}$ , we adopt Eq. 7 as the definition of an effective Born radius,  $a$ .

The electrostatic component of the transfer free energy into the nanotube (columns labeled MD; Table 3) is obtained as the difference between the charging free energies in nanotube (Table 2) versus bulk (Table 1). It is clear that

**TABLE 2** Excess free energy (in kcal/mol) for charging the ion in nanotube mid- and  $\alpha$ -planes

Ion	Midplane			$\alpha$ -Plane		
	MD	Model A	Model B	MD	Model A	Model B
Li <sup>+</sup>	-129.5 $\pm$ 2	-110.1	-137.4	-120.5 $\pm$ 1	-109.7	-130.4
Na <sup>+</sup>	-105.3 $\pm$ 1	-92.9	-113.2	-106.7 $\pm$ 3	-92.5	-110.4
Rb <sup>+</sup>	-71.1 $\pm$ 1	-66.8	-79.7	-78.6 $\pm$ 3	-64.5	-84.5
Cl <sup>-</sup>	-70.8 $\pm$ 3	-87.7	-90.5	-82.0 $\pm$ 1	-88.2	-96.8

MD, Molecular dynamics; Models A and B, macroscopic models discussed in the text. For the macroscopic calculations the grid level is  $51 \times 1.0:101 \times 0.1$ .

the cations tend to partition readily into the tube, whereas the anion does not. This trend is in agreement with experimental observations (Sanchez-Quesada and Ghadiri, personal communication). There are two reasons for the favorable partitioning of the cations: enhanced ion-water interaction and favorable interaction of the cation with the nanotube. The issue of ion-water interaction is addressed below, and the role of nanotube-ion interaction is addressed in the Discussion section.

The radial distribution of water around the ions (Fig. 2) indicates that the first shell is somewhat narrower around the ion inside the nanotube than in the bulk. This indicates more tightly bound water molecules in the channel. On the other hand, in comparison with bulk, the first shell in the channel has fewer water molecules, indicating desolvation (Table 4). The coordination number is determined from the integral of the radial distribution function. The angular distribution of water dipoles around the ion is a subtler metric of ion-water interaction (for example, see Jayaram et al., 1989; Hyun et al., 1995). In the channel midplane (Fig. 3), for Li<sup>+</sup> and Na<sup>+</sup>, the water around the ion in the nanotube is more highly structured than in bulk with angles mostly confined to very favorable dipole orientations ( $\cos \theta > 0.75$ ), whereas for Rb<sup>+</sup> in the midplane distribution of dipoles is bulk-like. In the channel  $\alpha$ -plane (Fig. 3) the distribution is bulk-like for Li<sup>+</sup>, whereas enhanced structuring is observed for Na<sup>+</sup> and Rb<sup>+</sup>. Similar calculations at a charge state of  $\lambda = 0.5$  indicates that the angular distribution of water dipoles around ions of all types are similar in the bulk and inside the nanotube (data not shown). Thus,

**TABLE 3** Calculated transfer free energies (in kcal/mol) from bulk to the nanotube

Ion	Midplane			$\alpha$ -Plane		
	MD	Model A	Model B	MD	Model A	Model B
Li <sup>+</sup>	-19.0 $\pm$ 2	0.4	-26.9	-10.0 $\pm$ 1	0.8	-19.9
Na <sup>+</sup>	-11.8 $\pm$ 1	0.6	-19.7	-13.2 $\pm$ 3	1.0	-16.9
Rb <sup>+</sup>	-5.0 $\pm$ 1	0.3	-12.6	-11.5 $\pm$ 3	2.6	-17.4
Cl <sup>-</sup>	24.0 $\pm$ 3	7.1	4.3	12.8 $\pm$ 1	6.6	-2.0

Rest as in Table 2.

**TABLE 4** First shell coordination number  $N_{\text{coord}}$  of the ions in the tube and in the bulk

Ion	Exptl.	Bulk	Midplane	$\alpha$ -Plane
Li <sup>+</sup>	4–6	5	5	4
Na <sup>+</sup>	4–8	5.8	4	4
Rb <sup>+</sup>	—	7.0	4	4.9
Cl <sup>-</sup>	6–8	7.5	4	5.6

The values are obtained from the integral of  $g(r)$ . The experimental hydration numbers are for the ion in the bulk (Marcus, 1985) and the other values are from the simulations.  $N_{\text{coord}}$  is based on the number of nearest oxygen atoms.

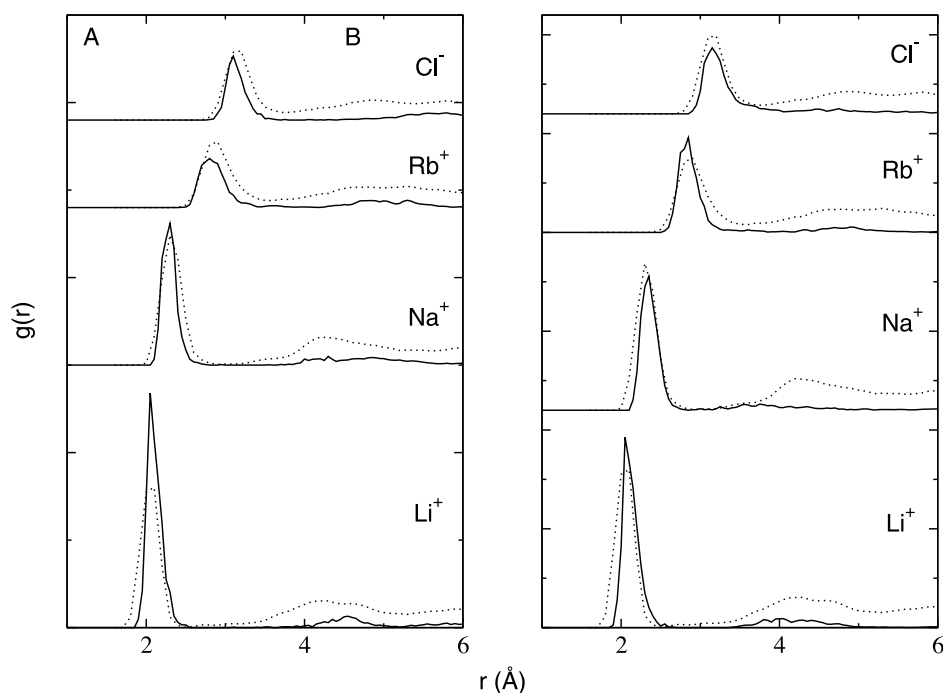
any structuring beyond that found in bulk appears when ion charges are above  $\sim 50\%$  of their full formal charge.

For Cl<sup>-</sup> (Fig. 3) in the channel midplane, the angular distribution of water is quite different from the bulk. In the bulk the angular distribution peaks around  $\cos \theta \approx -0.6$ . This corresponds to a linear hydrogen bond between Cl<sup>-</sup> and water (see Solvation structure in theory and methods). This means that in bulk, the bifurcated hydrogen bond to the ion, corresponding to  $\cos \theta = -1$ , is less favored than the single H-bond that leaves the other H-atom free to H-bond with other water molecules. These results are consistent with those of Ichiye and coworkers (Hyun et al., 1995). (Their definition of  $\theta$  differs by  $\pi$  from our definition. Also, if we normalize our distributions (data not shown), the peak magnitudes are in the same range as theirs, but the agreement is not exact, as our Cl<sup>-</sup> parameters are somewhat different than theirs.) In contrast, the distribution in the nanotube midplane shows a large fraction of water molecules in the bifurcated hydrogen bond configuration. In the  $\alpha$ -plane, however, the angular distribution of water dipoles is similar to that for the ion in the bulk albeit with some skew toward the bifurcated H bond (Fig. 3).

The data points in Figs. 4 and 5 show the potential calculated using Eq. 5, i.e., the electrostatic response function both inside the nanotube and in the reference bulk solvent. These data are fit to quadratic functions of  $\lambda$  in the plots. However, the quadratic terms are much smaller than the linear terms, and the curves can be said to be nearly linear.

At the  $\lambda = 0$  state, the calculations predict a non-zero, positive potential at the site of the (uncharged) ion in bulk, consistent with results found by earlier investigators (Pratt et al., 1994; Hummer et al., 1996; Ashbaugh and Wood, 1997). The potential predicted at the site of Na<sup>+</sup> is  $\sim 9.0$  kcal/mol-e, in good agreement with the range of values observed by earlier investigators for particles of similar dimensions. As a test of our simulation protocol, we calculated  $\langle \psi \rangle_0$  at Na<sup>+</sup> in a box of SPC water molecules. The Na<sup>+</sup> ion potential parameters were those of Straatsma and Berendsen (1988). We get  $\langle \psi \rangle_0 = 10.3$  kcal/mol-e and  $\Delta A = -94.8$  kcal/mol, which agrees well with  $\langle \psi \rangle_0 = 10.1$  kcal/mol-e and  $\Delta A = -95.7 \pm 0.6$  kcal/mol-e reported by

FIGURE 2 Ion-oxygen (water) radial distribution function,  $g(r)$ , in bulk (dotted line) and inside the tube (solid line). (A) Ion in the midplane. (B) Ion in the  $\alpha$ -plane. The curves have been arbitrarily shifted along the ordinate to fit on the same graph and hence no values are specified for the ordinate. Inside the tube, the absence of a pronounced second maxima is an artifact of using a radial distribution function for waters that are constrained by the cylindrical geometry of the tube: beyond the first shell the  $g(r)$  has little meaning inside the tube. The raw distribution functions have been smoothed (Allen and Tildesley, 1997).



Ashbaugh and Wood (1997) using the same set of parameters (data not tabulated). Likewise, we calculate  $\langle\psi\rangle_1 = -164.7$  kcal/mol-e before and  $\langle\psi\rangle_1 = -215.3$  kcal/mol-e after finite-size correction (data not tabulated), respectively. These values are also in good agreement with those read from Fig. 1 in Ashbaugh and Wood (1997), further reinforcing our confidence in our calculations.

### Continuum electrostatics

The electrostatic component of the excess free energy of the ion inside the nanotube, calculated via two different macroscopic models, is shown in Table 2. These models are schematically illustrated in Fig. 6. Model A is the simplest: the water inside the nanotube is assumed to be a uniform medium

FIGURE 3 Probability distribution,  $p(\cos \theta)$ , of the orientation of water dipoles around the ions. Dotted lines, ion in bulk; solid line, ion in nanotube midplane; and broken line, ion in the nanotube  $\alpha$ -plane.

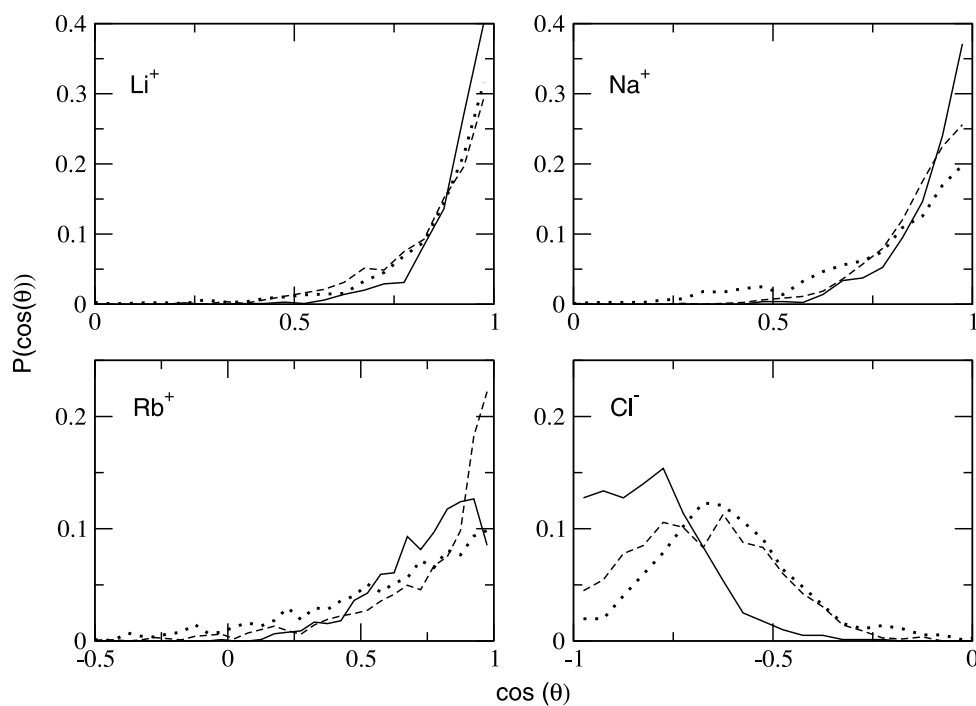
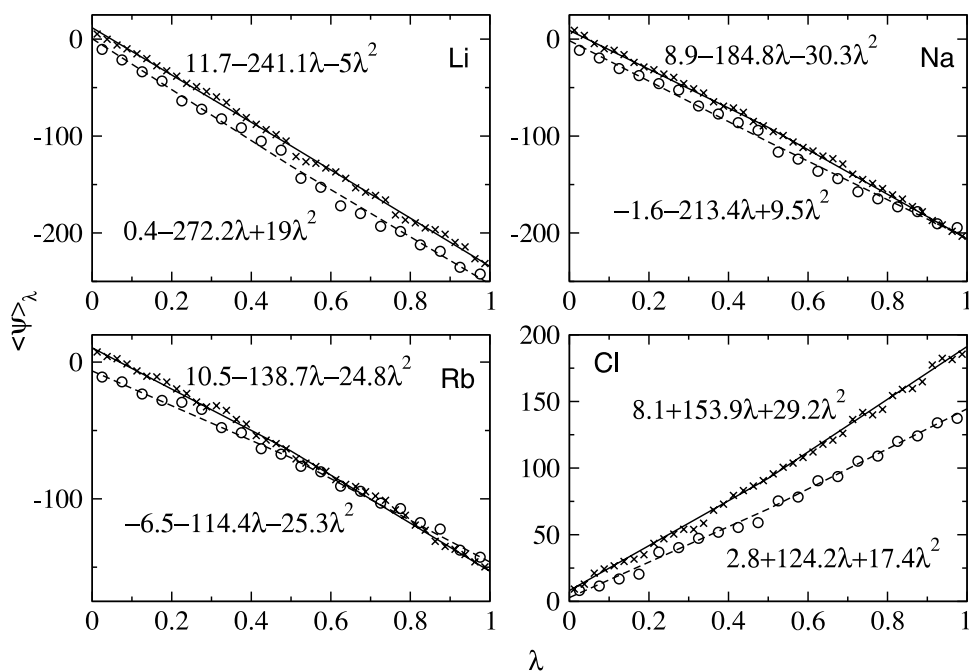


FIGURE 4 Average potential, Eq. 5, at the ion in the midplane at charge state  $\lambda$ . ( $\circ$ ), Ion in the nanotube; ( $\times$ ), ion in the bulk solvent. The solid line is least squares fit to the bulk data. The dashed line is least squares fit to the nanotube data. The fitted equations are also shown.

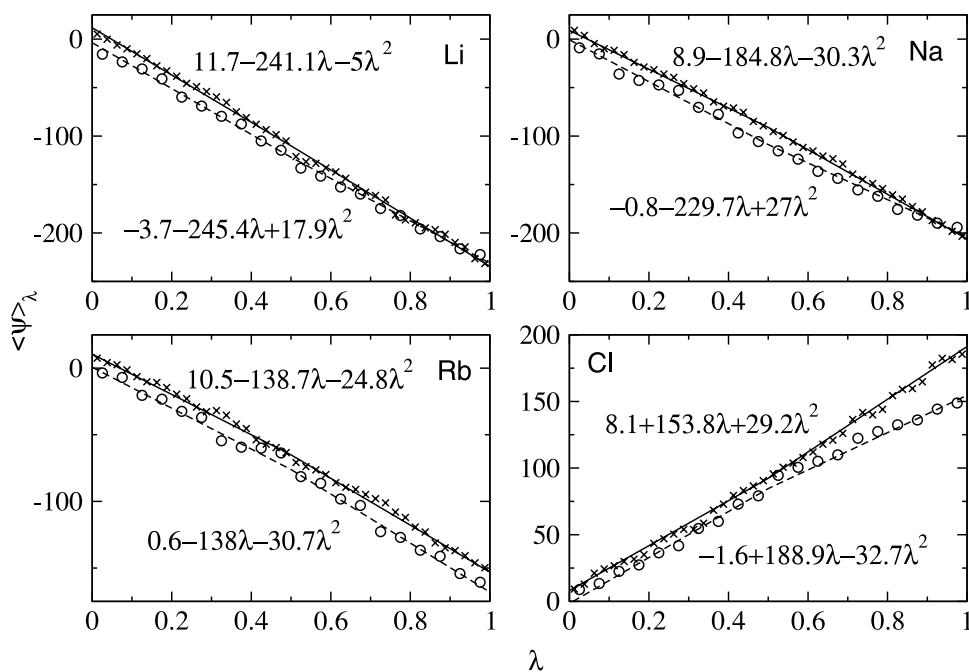


of dielectric constant 80. The ion radii are the Born radii from Table 1. Model B explicitly considers the first shell water molecules as part of the low-dielectric nanotube environment, i.e. in model B, the first-solvation shell water molecules are modeled atomistically and assigned  $\epsilon = 4$ , equal to dielectric constant of the nanotube. The water molecules beyond the first-solvation shell are described as a continuum of  $\epsilon = 80$ . The number of water molecules is set equal to the coordination number observed in the simulations (Table 4), and at each

charge state ( $\lambda = 0.25, 0.5, 0.75, 1.0$ ), the position of the water molecule is reoptimized to mimic the response of a molecular fluid instead of a continuous medium (see Methods).

Table 3 shows the calculated bulk to nanotube transfer free energies, and Figs. 7 and 8 depict the solvation free calculated via the continuum models against their atomistic counterpart. For  $\text{Li}^+$  and  $\text{Na}^+$  in the midplane and for  $\text{Na}^+$  and  $\text{Rb}^+$  in the  $\alpha$ -plane, model B describes the simulation results better than model A. (The difference between MD results and continuum

FIGURE 5 Average potential, Eq. 5, at the ion in the  $\alpha$ -plane. Rest as in Fig. 4.





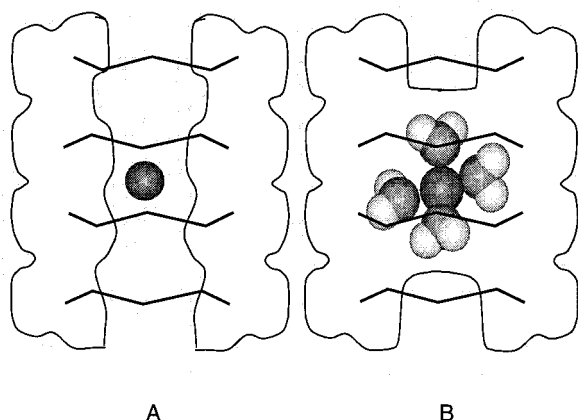


FIGURE 6 Models of ion solvation within the macroscopic formulation. The environment outside the tube has a dielectric constant of 80. Model A, channel lumen has a dielectric constant of 80; model B, explicit water molecules are included as part of the nanotube environment.

results are smaller for model B.) For  $\text{Li}^+$  in the  $\alpha$ -plane, models A and B have errors of approximately equal magnitude but opposite sign. For  $\text{Cl}^-$  both models A and B are inadequate for the ion in the midplane, and in the  $\alpha$ -plane model A better describes simulation results.

## DISCUSSION

We briefly discuss the bulk free energy calculations before addressing the main concerns of this work, namely the formulation of continuum models based on insights from simulations. As Table 1 illustrates, although the trends in the solvation free energies are similar to experimental estimates, there is disagreement in magnitude between our calculations using Ewald summation and those performed with ions in a water droplet surrounded by a vacuum (Åqvist, 1990; Beglov and Roux, 1994; Roux, 1996). Using Ewald summation, we find that the charging free energy for cations is  $\sim 10$  kcal/mol less negative than the corresponding value obtained in simulations using water droplets. For  $\text{Cl}^-$  the Ewald summation results are more negative by  $\sim 15$  kcal/mole than the corresponding values from water-droplet simulations. Darden et al. (1998) find a similar discrepancy and have suggested water polarization at the droplet-vacuum interface as a possible cause. Thus, although we use the same parameters, using Ewald electrostatics leads to numbers (predictably) different than those with droplet simulations. However, the relative trends are consistent between different methods. Likewise, for charging the ion in the nanotube, this difference between droplet simulations and our Ewald approach can be expected to hold. Thus, in calculating the free energy change for bulk to tube partitioning, both Ewald and droplet approaches should lead to similar results.

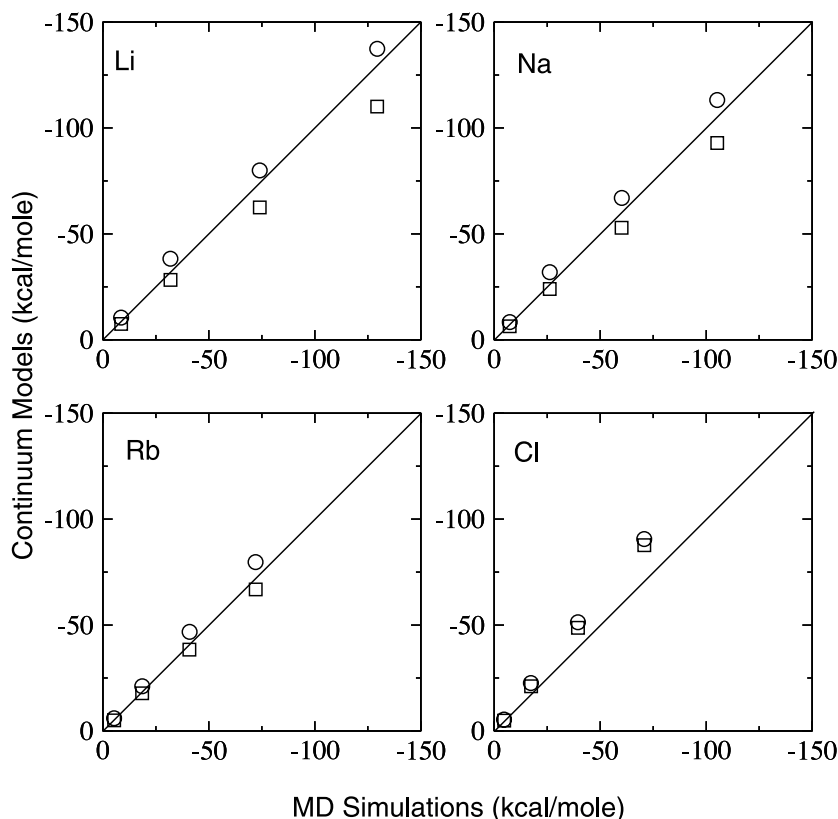


FIGURE 7 Comparison of free energies (kcal/mol) calculated via macroscopic models versus MD simulations for ion the mid-plane. ( $\square$ ), Model A; ( $\circ$ ), model B. In each panel, the charge states are successively  $\lambda = 0.25, 0.5, 0.75$ , and  $1.00$  from bottom left-hand corner to top right-hand corner.

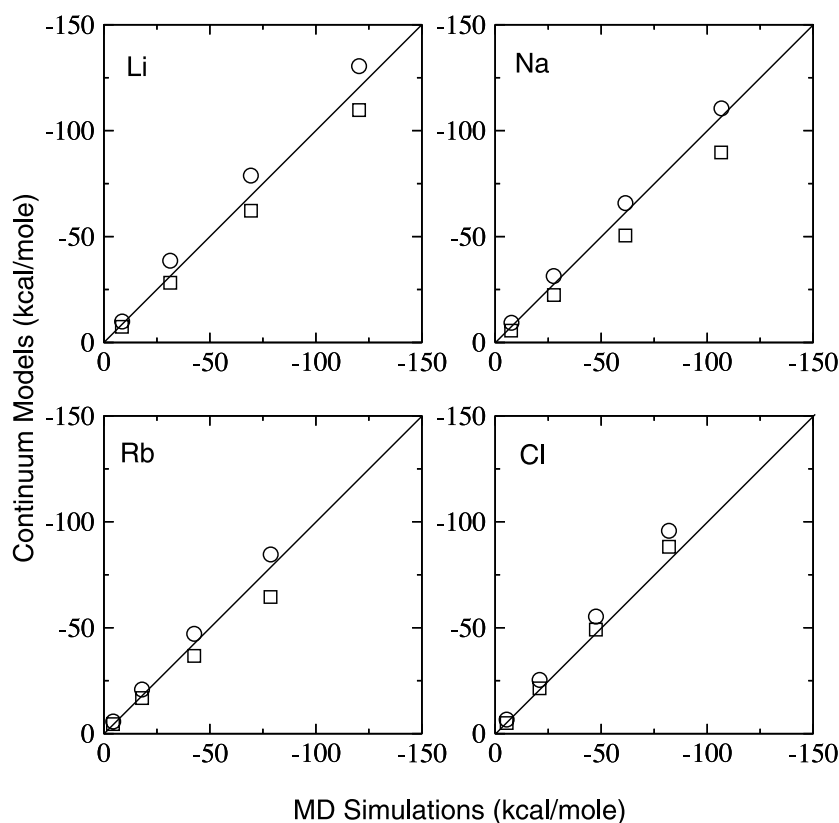


FIGURE 8 Comparison of free energies (kcal/mol) calculated via macroscopic models versus MD simulations for ion the  $\alpha$ -plane. Rest as in Fig. 7.

This is heartening, as to the best of our knowledge the Ewald-electrostatics approach for charging ions in nanotubes is novel and the trends obtained using a different method would be similar to those presented in this paper.

As Table 3 indicates, cation partitioning is favored into the nanotube. As cation size is increased, the partitioning free energy is reduced. Experimentally,  $K_m$ , the affinity constant, for ion-nanotube interactions suggests that  $\text{Li}^+$  readily partitions into the nanotube,  $\text{Na}^+$  does to a lesser extent followed by  $\text{Rb}^+$  (Sanchez-Quesada and Ghadiri, personal communication). This trend is validated by our MD simulations (Table 3).

The role of the nanotube in determining the changes in free energies for transition from the mid- to  $\alpha$ -plane is two-fold. One aspect is the nanotube's influence on ion water interactions and the second is the interaction of the ion with nanotube partial charges. Engels et al. (1995) have shown that the water occupancy of an ion-free nanotube is  $\sim$ two to three water molecules in the midplane and  $\sim$ one to two water molecules in the  $\alpha$ -plane. These numbers reflect how much space there is to accommodate water molecules in each zone, and the observed coordination numbers and the attendant changes in free energies can be considered in this light.

$\text{Li}^+$  in the midplane coordinates with  $\sim$ five water molecules (Table 4), three within the midplane region and one each from the  $\alpha$ -plane above and below. In the  $\alpha$ -plane, one

might guess that  $\text{Li}^+$  would coordinate with six waters, three each from the adjacent midplanes. However, the calculated value is four, two each from the adjacent midplanes. It is likely that tighter coordination with fewer water molecules is preferred over the converse. Clearly a loss of one water molecule influences the less favorable free energy of solvation in the  $\alpha$ -plane (Table 3). For  $\text{Na}^+$  there is no change in the coordination number in going from mid- to  $\alpha$ -plane (Table 4), and the change in free energy in going from mid- to  $\alpha$ -plane is not as great (Table 3). For  $\text{Na}^+$ , the midplane to  $\alpha$ -plane transition energy is consistent with earlier studies by Demchuk and Bashford using a completely different umbrella-sampling technique (unpublished observations). The smaller  $N_{\text{coord}}$ , in comparison with  $\text{Li}^+$ , in the midplane is likely due to the larger size of particle. For  $\text{Na}^+$  in the  $\alpha$ -plane, as for  $\text{Li}^+$ , it appears that a smaller, tightly coordinated first shell is preferred. For  $\text{Rb}^+$ ,  $N_{\text{coord}}$  increases in the  $\alpha$ -plane (Table 4) and the free energy change in going from mid- to  $\alpha$ -planes is also favorable (Table 3). A similar trend is seen for  $\text{Cl}^-$  (Tables 3 and 4), and the sharp change in free energy in going from midplane to  $\alpha$ -plane is again consistent with the calculations by Demchuk and Bashford (unpublished observations).

The role of the direct nanotube-ion interaction can be seen by decomposing  $\psi_{\text{channel}}$  from model B into contributions from the first solvation-shell water molecules,  $\psi_{\text{water}}$ , and the nanotube,  $\psi_{\text{tube}}$  (Table 5). The changes in free

**TABLE 5** Decomposition of the electrostatic potential (in kcal/mol-e) on the ion within model B

Ion	Midplane			$\alpha$ -Plane		
	$\psi_{\text{tube}}$	$\psi_{\text{water}}$	$\psi_{\text{rxn}}$	$\psi_{\text{tube}}$	$\psi_{\text{water}}$	$\psi_{\text{rxn}}$
Li	-8.1	-39.8	-179.0	-5.3	-34.9	-180.2
Na	-7.9	-28.3	-153.8	-5.2	-28.3	-153.8
Rb	-8.3	-15.3	-112.2	-5.4	-22.7	-113.0
Cl	-5.6	19.1	154.0	-3.5	22.2	155.2

$\psi_{\text{tube}}$ , Potential due to the nanotube charges;  $\psi_{\text{water}}$ , potential due to water charges.  $\psi_{\text{water}} + \psi_{\text{tube}} = \psi_{\text{channel}}$  in Eq. 6.  $\psi_{\text{rxn}}$  is the reaction potential acting on the source (ion) charge. Note that in magnitude  $\psi_{\text{rxn}}$  for the ion in bulk solvent is just twice the solvation free energy reported in Table 1.

energy suggested by changes in coordination number are validated by the changes in  $\psi_{\text{water}}$ : increased coordination numbers are reflected in more favorable ion water interactions. Further,  $\psi_{\text{tube}}$  is uniformly negative throughout the channel. This clearly influences the preferential solvation of cations inside the tube. Also  $\psi_{\text{tube}}$  decreases in magnitude from the mid- to the  $\alpha$ -plane. This is due to the diminished effect of the negatively charged carbonyl oxygens lining the midplane and an enhanced effect of the positively charged  $C_{\alpha}$  atoms.

Table 5 also reveals expected trends for  $\psi_{\text{rxn}}$ , the energetic response of the dielectric. For  $\text{Na}^+$  and  $\text{Cl}^-$ , the Born radii are nearly equal, and correspondingly  $\psi_{\text{rxn}}$  is also nearly equal, but opposite in sign. Further, the Born equation, Eq. 7, suggests that  $\psi_{\text{rxn}}$  should be larger for smaller radii, as is seen in Table 5. Finally, on account of desolvation and because of the low dielectric nanotube, the reaction field component of the free energy would be less negative inside the nanotube; correspondingly  $(1/2)\psi_{\text{rxn}}q$  is less negative than the bulk value (Table 1) as expected.

We emphasize that in our calculations, the ion does not have a contact interaction with the peptide channel (Fig. 1), as it is always restrained near the axis of the channel. That such a calculation is credible is seen from the calculations by Crozier et al. (2001). In their simulations of a model channel of diameter 8.1 Å, it is seen that the ion hardly moves farther than 1 Å from the channel axis. This study is relevant to the present discussion, as the choice of dipoles lining the channel wall and the chosen diameter are similar to that in the nanotube.

### Macroscopic models and simulations

Model A is a purely linear response model because 1) the water inside the tube is described as a continuum dielectric and 2) the nanotube has a fixed structure. The simulations in the bulk and in the nanotube suggest some deviation from linearity (Figs. 4 and 5), but the nonlinearity is quite modest. Hence, our intuitive expectation would be that a linear response model would hold for the ion in the bulk and in the nanotube. However, calculations with model A belie this

**TABLE 6** Calculated root mean square error for free energies of charging calculated via model A and model B in the midplane

Charge limit		Model A	Model B	Solvent structuring
Li	High	15.9	7.1	Structured
	Low	2.7	4.7	
Na	High	10.1	7.4	Structured
	Low	1.7	4.1	
Rb	High	4.1	6.8	Bulk-like
	Low	0.5	2.0	
Cl	High	13.6	16.2	Skewed
	Low	2.6	3.7	

The reference values are from MD simulations (Table 2). The rms error is calculated separately for the high-charge (see text) and low-charge limits. Solvent refers to the first-shell water molecules. In the low-charge limit, solvent structuring is always bulk-like.

expectation. In some instances the model A results are closer to MD and in others the model B results are closer. Below we reconcile this observation with information obtained from simulations. To facilitate the discussion we refer to the  $\lambda = 0.75, 1.0$  states as the high-charge limit, and the  $\lambda = 0.25, 0.5$  states as the low-charge limit.

Tables 6 and 7 shows the deviations of models A and B from the simulation results. In the low-charge limit it is seen that model A almost always describes the simulated trends better than model B. In this limit, as we noted earlier, the solvent structuring around the ion is bulk-like. Further, the solvent is fairly disordered when ion charges are low (data not shown; see Jayaram et al., 1989). Hence, in the low-charge limit either model B is inappropriate or using a low dielectric constant for the first shell water is inappropriate. This conclusion is similar to that reached by Partenskii and Jordan (1992a,b). They find that in the low-field limit the dipolar chain in their model of an ion-channel with a single file of water has a high dielectric constant. In their model the low field limit is for ion charges less than 20 to 30% of their full formal value, a reflection of the single file of water; a wider channel should shift this limit higher, as it does in the nanotube.

For the cations in the midplane, Fig. 3 indicates that in the high-charge limit, the first solvation shell around  $\text{Li}^+$  and

**TABLE 7** Calculated root mean square error for free energies of charging calculated via model A and model B in the  $\alpha$ -plane

Charge limit		Model A	Model B	Solvent
Li	High	9.1	9.7	Bulk-like
	Low	2.3	5.2	
Na	High	14.2	4.1	Structured
	Low	4.0	2.9	
Rb	High	10.8	5.3	Structured
	Low	0.9	2.1	
Cl	High	4.5	11.2	Bulk-like
	Low	0.5	3.2	

Rest as in Table 6.

$\text{Na}^+$  is structured, whereas it is bulk-like for  $\text{Rb}^+$ . Correspondingly, in this limit, for  $\text{Li}^+$  and  $\text{Na}^+$  model B describes the data better (Table 6 and Fig. 7) and model A does so for  $\text{Rb}^+$ . In the  $\alpha$ -plane, the solvent around  $\text{Li}^+$  is bulk-like, whereas it is more structured around  $\text{Na}^+$  and  $\text{Rb}^+$ . Correspondingly, for  $\text{Li}^+$  model A best describes the data in the high-charge limit, and model B does so for  $\text{Na}^+$  and  $\text{Rb}^+$  (Table 7 and Fig. 8).

$\text{Cl}^-$  solvation provides an interesting counterpoint to the studies with cations. For the cations, the hydrogen bonding pattern with water is similar for the ion in the bulk and in the nanotube, only the magnitude of ordering changes. For  $\text{Cl}^-$  in the midplane, the orientational ordering of water is much different than that seen in bulk with a trend towards bifurcated hydrogen bonding with water (Fig. 3). In the high-charge limit, model B is clearly a poor descriptor of solvation and so is model A (Fig. 7 and Table 6). This is understandable in light of the fact that the Born radius was calculated with linear hydrogen bonding dominant. It may indeed be appropriate to recalculate a Born radius for solvation via bifurcated hydrogen bonds, but we have not undertaken this task as our aim was to formulate a consistent model with a limited number of adjustable parameters. The above point about redefining Born radii becomes clearer when one considers the solvation of  $\text{Cl}^-$  in the  $\alpha$ -plane. Here the orientational ordering is fairly similar to that seen in the bulk solvent (Fig. 3), and because no pronounced structuring is seen, model A might be expected to describe the MD trends better. Indeed this is what is seen (Fig. 8 and Table 7).

In the above analysis, we have tried to correlate the trends from continuum models with solvent structuring. Since saturation (nonlinearity) in electrostatic response must go hand-in-hand with increase in structural ordering, the lack of a significant nonlinearity in the calculated response (Figs. 4 and 5) is somewhat unanticipated. One plausible explanation is that inaccuracies in our simulation mask any nonlinearity. Thus, when the linearity or nonlinearity of the electrostatic response is unable to provide a clear direction in the choice of continuum models, the structural calculations appear to be better guides in choosing an appropriate continuum model.

Thus, of our simulation approaches, one gives us structural information regarding ion solvation, and these simulations can be performed with relative ease. Based on these simulations, if one finds enhanced structuring of water around the ion relative to bulk values, then it is fair to expect a model like our model B to be a better model for describing the solvation thermodynamics. This is a principal result of our paper. The other simulations are computationally more expensive perturbation free energy calculations. These simulations can be analyzed to understand the electrostatic response, and based on that one can construct appropriate continuum models (see Jayaram et al., 1989). However, in the present case, we find that due to likely inaccuracies in

our simulations, it is difficult to use the electrostatic response (a derivative of a free energy) as a sole guide in the formulation of continuum models.

### Choice of dielectric constants

In our continuum electrostatic calculations, the only free parameter is the assumed dielectric constant of the nanotube and the first shell water molecules, the peptide charges and radius parameters having been determined from PARAM22 and the ion Born radii from the bulk simulations, respectively. The calculations discussed above were all performed with this dielectric constant set to 4. Calculations with dielectric constants of 3 and 5 have also been done (data not shown). In all these cases, the qualitative trends predicted are as discussed earlier. Quantitative differences, however, exist: With a dielectric constant of 3 model B uniformly overpredicts solvation, but the differences are all within 5 kcal/mol. Similarly with a dielectric constant of 5, the values are uniformly underpredicted.

The assignment of a low dielectric constant to the first solvation shell water molecules is based on their being partially immobilized, as evidenced by the dipole distributions. In particular, model B, in which the first-shell water and the peptide are assigned the same low dielectric constant, represents an assumption that the first-shell water dipoles are immobilized to approximately the same extent as the peptide dipoles. Interestingly, in the high-field/high-charge limit Jordan and coworkers (Partenskii and Jordan, 1992a,b) find that the dipolar chain in their model of the ion channel is best described with a dielectric constant between 3 and 5, a value that also depends on the location of the ion inside the tube. This is so because in the high field limit the dipolar chain is nearly immobilized.

Proteins often have been modeled as media of dielectric constant 4. This choice has found support in theoretical estimates of dielectric constants (Gilson and Honig, 1986; Simonson et al., 1991; Smith et al., 1993; Simonson, 1999; Pitera et al., 2001). The internal dielectric constant of proteins, accounting only for the fluctuation of the amide dipoles and backbone conformation, is between 2 and 5 (Gilson and Honig, 1986; Simonson et al., 1991; Smith et al., 1993; Pitera et al., 2001), whereas including charged side-chain motion increases the value to between 15 and 25 (Smith et al., 1993; Simonson, 1999; Pitera et al., 2001). Because the nanotube system is restrained and also has no free charged side chain residues, the dielectric constant is expected to be in the vicinity of 2 to 5.

### CONCLUSIONS

The nanotube environment confines the ion and water and this leads to either enhanced structuring of water around the ion or, when there is enough "wiggle" room, the solvent



structure around the ion is bulk-like. This is true for the cations. For  $\text{Cl}^-$ , the interaction with water tends to be much different from that seen in bulk: linear hydrogen bonding in bulk versus bifurcated hydrogen bonding for the ion in the midplane of the nanotube. In the  $\alpha$ -plane, where  $\text{Cl}^-$  coordinates with more water molecules, the interaction with water is more bulk-like.

When enhanced structuring around the ion is observed, the continuum model, with parameters based on bulk solvent simulations, is improved if the first solvation shell water is treated explicitly as part of the low dielectric protein environment. If solvation structure is bulk-like, no advantage results in treating the first solvation shell explicitly. The results with  $\text{Cl}^-$  add a cautionary note to this conclusion. If the geometry of interaction with solvent is much different in the tube versus the bulk, then either of the above approaches is likely to fail, as is the case with  $\text{Cl}^-$  in the midplane. In this regard, it would be interesting to study  $\text{Cl}^-$  selective channels and consider how cations behave in them.

Solvent ordering must be accompanied by changes in its electrostatic response. However, within the accuracies of the simulation, we find that the electrostatic response is nearly linear both in the bulk and inside the nanotube. Thus, in the absence of an unequivocal result from the electrostatic response, it appears best to use solvent structural information in formulating continuum models of solvation inside nanotubes.

Our work suggests a plausible facile route to study ion solvation in channel systems. One could perform a few dynamical simulations to estimate the disposition of water about the ion. This information can then be used to construct continuum models along the lines suggested in this work. These models can be used to calculate the free energy of charging at a much lower computational cost than MD-based free energy methods.

We gratefully acknowledge funding from the Office of Naval Research (N00014-95-1-1293). We thank Drs. Reza Ghadiri and Jorge Sanchez-Quesada for helpful discussion and for sharing experimental data prior to publication.

## REFERENCES

- Allen, M. P., and D. J. Tildesley. 1997. *Computer simulation of liquids*. Oxford University Press, New York.
- Åqvist, J. 1990. Ion-water interaction potentials derived from free energy perturbation simulations. *J. Phys. Chem.* 94:8021–8024.
- Åqvist, J., and V. Luzhkov. 2000. Ion permeation mechanism of the potassium channel. *Nature*. 404:881–884.
- Åqvist, J., and A. Warshel. 1989. Energetics of ion permeation through membrane channels. *Biophys. J.* 56:171–182.
- Arseniev, A. S., V. F. Bystrov, T. V. Ivanov, and Y. A. Ovchinnikov. 1985.  $^1\text{H}$ -NMR study of gramicidin-a transmembrane ion channel: head-to-head right handed single stranded helices. *FEBS Lett.* 186:168–174.

- Ashbaugh, H. S., and R. H. Wood. 1997. Effects of long-range electrostatic potential truncation on the free energy of ionic hydration. *J. Chem. Phys.* 106:8135–8139.
- Babu, C. S., and C. Lim. 1999. Theory of ionic hydration: insights from molecular dynamics simulations and experiment. *J. Phys. Chem. B.* 103:7958–7968.
- Bashford, D. 1997. An object-oriented programming suite for electrostatic effects in biological molecules. In *Scientific Computing in Object-Oriented Parallel Environments: Lecture Notes in Computer Science*, Volume 1343. Y. Ishikawa, R. R. Oldehoeft, and J. V. W. Reinders, editors. Springer, Berlin. 233–240.
- Bashford, D., and K. Gerwert. 1992. Electrostatic calculations of the pKa values of ionizable groups in bacteriorhodopsin. *J. Mol. Biol.* 224:473–486.
- Bayley, H. 1999. Designed membrane channel and pores. *Curr. Opin. Biotechnol.* 10:94–103.
- Beglov, D., and B. Roux. 1994. Finite representation of an infinite bulk system: solvent boundary potential for computer simulations. *J. Chem. Phys.* 100:9050–9063.
- Berendsen, H. J. C., J. P. M. Postma, W. F. van Gunsteren, A. DiNola, and J. R. Haak. 1984. Molecular dynamics with coupling to an external bath. *J. Chem. Phys.* 81:3684–3690.
- Bernéche, S., and B. Roux. 2000. Molecular dynamics of KcsA  $\text{K}^+$  channel in a bilayer membrane. *Biophys. J.* 78:2900–2917.
- Beveridge, D. L., and F. M. DiCupua. 1989. Free energy via molecular simulation. *Ann. Rev. Biophys. Biophys. Chem.* 18:431–492.
- Born, M. 1920. Volumen und hydrationswärme der ionen. *Zeits. Physik.* 1:45–48.
- Brooks, B. R., R. E. Bruccoleri, B. D. Olafson, D. J. States, S. Swaminathan, and M. Karplus. 1983. CHARMM: a program for macromolecular energy, minimization, and dynamics calculations. *J. Comp. Chem.* 4:187–217.
- Connolly, M. 1983. Analytical molecular surface calculation. *J. App. Crystogr.* 16:548–558.
- Crozier, P. S., R. L. Rowley, N. B. Holladay, D. Henderson, and D. D. Busath. 2001. Molecular dynamics simulation of continuous current flow through a model biological membrane channel. *Phys. Rev. Lett.* 86:2467–2470.
- Darden, T., D. Pearlman, and L. Pedersen. 1998. Ionic charging free energies: spherical versus periodic boundary conditions. *J. Chem. Phys.* 109:10921–10935.
- Engels, M., D. Bashford, and M. R. Ghadiri. 1995. Structure and dynamics of self-assembling peptide nanotubes and the channel-mediated water organization and self-diffusion: a molecular dynamics study. *J. Am. Chem. Soc.* 117:9151–9158.
- Feller, S. E., R. W. Pastor, A. Rojnuckarin, S. Bogusz, and B. R. Brooks. 1996. Effect of electrostatic force truncation on interfacial and transport properties of water. *J. Phys. Chem.* 100:17011–17020.
- Fernandez-Lopez, S., H.-S. Kim, E. C. Choi, M. Delgado, J. R. Granja, A. Khasanov, K. Kraehenbuehl, G. Long, D. A. Weinberge, K. M. Wilcoxen, and M. R. Ghadiri. 2001. Antibacterial agents based on the cyclic (D,L)- $\alpha$ -peptide architecture. *Nature*. 412:452–455.
- Figureirido, F., G. S. D. Buono, and R. M. Levy. 1994. Molecular mechanics and electrostatic effects. *Biophys. Chem.* 51:235–241.
- Ghadiri, M. R., J. R. Granja, and L. K. Buehler. 1994. Artificial transmembrane ion channels from self-assembling peptide nanotubes. *Nature*. 369:301–304.
- Ghadiri, M. R., J. R. Granja, R. A. Milligan, D. E. McRee, and N. Khazanovich. 1993. Self-assembling organic nanotubes based on a cyclic peptide architecture. *Nature*. 366:324–327.
- Gilson, M. K., and B. H. Honig. 1986. The dielectric constant of a folded protein. *Biopolymers*. 25:2097–2119.
- Hao, Y., M. R. Pear, and D. D. Busath. 1997. Molecular dynamics study of free energy profiles for organic cations in gramicidin channels. *Biophys. J.* 73:1699–1716.
- Hartgerink, J. D., T. D. Clark, and M. R. Ghadiri. 1998. Peptide nanotubes and beyond. *Chem. Euro. J.* 4:1367–1372.

- Hummer, G., L. R. Pratt, and A. E. García. 1996. Free energy of ionic hydration. *J. Phys. Chem.* 100:1206–1215.
- Hummer, G., and A. Szabo. 1996. Free energy differences from computer simulations of initial and final states. *J. Chem. Phys.* 105:2004–2010.
- Hyun, J. K., C. S. Babu, and T. Ichiye. 1995. Apparent local dielectric response around ions in water: a method for its determination and its applications. *J. Phys. Chem.* 99:5187–5195.
- Jayaram, B., R. Fine, K. Sharp, and B. Honig. 1989. Free energy calculations of ion hydration: an analysis of the born model in terms of microscopic simulations. *J. Phys. Chem.* 93:4320–4327.
- Jorgensen, W., J. Chandrasekhar, J. D. Madura, R. W. Impey, and M. L. Klein. 1983. Comparison of simple potential functions for simulating liquid water. *J. Chem. Phys.* 79:926–935.
- Latimer, W. M., K. S. Pitzer, and C. M. Slansky. 1939. The free energy of hydration of gaseous ions, and the absolute potential of the normal calomel electrode. *J. Chem. Phys.* 7:108–111.
- MacKerell Jr., A. D., D. Bashford, M. Bellott, R. L. Dunbrack Jr., J. D. Evanseck, M. J. Field, S. Fischer, J. Gao, H. Guo, S. Ha, D. Joseph-McCarthy, L. Kuchnir, K. Kuczera, F. T. K. Lau, C. Mattos, S. Michnick, T. Ngo, D. T. Nguyen, B. Prod'homme, I. W. E. Reiher, III, B. Roux, M. Schlenkerich, J. C. Smith, R. Stote, J. Straub, M. Watanabe, J. Wiorkiewicz-Kuczera, D. Yin, and M. Karplus. 1998. All-atom empirical potential for molecular modeling and dynamics studies of proteins. *J. Phys. Chem. B.* 102:3586–3616.
- Marcus, Y. 1985. *Ion Solvation*. Wiley, London.
- Motesharei, K., and M. R. Ghadiri. 1997. Diffusion-limited size-selective ion sensing based on SAM-supported peptide nanotubes. *J. Am. Chem. Soc.* 119:11306–11312.
- Neria, E., S. Fischer, and M. Karplus. 1996. Simulation of activation energies in molecular systems. *J. Chem. Phys.* 105:1902–1921.
- Nina, M., D. Beglov, and B. Roux. 1997. Atomic radii for continuum electrostatics calculations based on molecular dynamics free energy simulations. *J. Phys. Chem. B.* 101:5239–5248.
- Opella, S. J., F. M. Marassi, J. J. Gesell, A. P. Valente, Y. Kim, M. Oblatt-Montal, and M. Montal. 1999. Structures of the M2 channel-lining segments from nicotinic acetylcholine and NMDA receptors by NMR spectroscopy. *Nat. Struct. Biol.* 6:374–379.
- Partenskii, M. B., V. Dorman, and P. C. Jordan. 1994. Influence of a channel-forming peptide on energy barriers to ion permeation, viewed from a continuum dielectric perspective. *Biophys. J.* 67:1429–1438.
- Partenskii, M. B., and P. C. Jordan. 1992a. Nonlinear dielectric behavior of water in transmembrane ion channels: ion energy barriers and the channel dielectric constant. *J. Phys. Chem.* 96:3906–3910.
- Partenskii, M. B., and P. C. Jordan. 1992b. Theoretical perspectives on ion-channel electrostatics: continuum and microscopic approaches. *Q. Rev. Biophys.* 25:477–510.
- Pitera, J. W., M. Falta, and W. F. van Gunsteren. 2001. Dielectric properties of proteins from simulation: the effects of solvent, ligands, pH, and temperature. *Biophys. J.* 80:2546–2555.
- Pratt, L. R., G. Hummer, and A. E. García. 1994. Ion pair potentials-of-mean-force in water. *Biophys. Chem.* 51:147–165.
- Rick, S. W., and B. J. Berne. 1994. The aqueous solvation of water: a comparison of continuum methods with molecular dynamics. *J. Am. Chem. Soc.* 116:3949–3954.
- Roux, B. 1996. Valence selectivity of the gramicidin channel: a molecular dynamics free energy perturbation study. *Biophys. J.* 71:3177–3185.
- Roux, B., and M. Karplus. 1991. Ion transport in a model gramicidin channel. *Biophys. J.* 59:961–981.
- Roux, B., and M. Karplus. 1993. Ion transport in the gramicidin channel: free energy of the solvated right-handed dimer in a model membrane. *J. Am. Chem. Soc.* 115:3250–3262.
- Roux, B., and R. MacKinnon. 1999. The cavity and pore helices in the KcsA K<sup>+</sup> channel: electrostatic stabilization of monovalent cations. *Science*. 285:100–102.
- Roux, B., H. A. Yu, and M. Karplus. 1990. Molecular basis for the born model of ion solvation. *J. Phys. Chem.* 94:4683–4688.
- Ryckaert, J. P., G. Cicotti, and H. J. C. Berendsen. 1977. Numerical integration of the cartesian equations of motion of a system with constraints: molecular dynamics of *n*-alkanes. *J. Comp. Phys.* 23:327–341.
- Sancho, M., M. B. Partenskii, V. Dorman, and P. C. Jordan. 1995. Extended dipole chain model for ion channels: electrostriction effects and the translocation energy barrier. *Biophys. J.* 68:427–433.
- Simonson, T. 1999. Dielectric relaxation in proteins: microscopic and macroscopic models. *Intl. J. Quant. Chem.* 73:45–57.
- Simonson, T., D. Perahia, and A. T. Brünger. 1991. Microscopic theory of the dielectric properties of proteins. *Biophys. J.* 59:670–690.
- Smart, O. S., J. M. Goodfellow, and B. A. Wallace. 1993. The pore dimensions of gramicidin A. *Biophys. J.* 65:2455–2460.
- Smith, P. E., R. M. Brunne, A. E. Mark, and W. F. van Gunsteren. 1993. Dielectric properties of trypsin inhibitor and lysozyme calculated from molecular dynamics. *J. Phys. Chem.* 97:2009–2014.
- Straatsma, T. P., and H. J. C. Berendsen. 1988. Free energy of ionic hydration: analysis of a thermodynamic integration technique to evaluate free energy differences by molecular dynamics simulations. *J. Chem. Phys.* 89:5876–5886.
- Tieleman, D. P., and H. J. C. Berendsen. 1998. A molecular dynamics study of the pores formed by *Escherichia coli* OmpF porin in a fully hydrated palmitoylphosphatidylcholine bilayer. *Biophys. J.* 74:2786–2801.
- Tosi, M. P. 1964. Appendix A: evaluation of electrostatic lattice potentials by the ewald method. In *Solid State Physics*, Volume 16. F. Seitz and D. Turnbull, editors. Academic Press, New York. 107–113.
- Zwanzig, R. W. 1954. High temperature equation of state by a perturbation method. *J. Chem. Phys.* 22:1420–1426.